CORA Cork Open Research Archive
Cartlann Taighde Oscailte Chorcaí

Title	Realization of high efficiency ultrasound-powered micro-LEDs for optogenetics
Authors	Mondal, Tanmay;Laursen, Kjeld;Hosseini, Seyedsina;Rashidi, Amin;Moradi, Farshad;Corbett, Brian
Publication date	2020-04-02
Original Citation	Mondal, T., Laursen, K., Hosseini, S., Rashidi, A., Moradi, F. and Corbett, B. (2020) 'Realization of high efficiency ultrasound-powered micro-LEDs for optogenetics', SPIE Photonics Europe, Strasbourg, France, 29 March - 2 April, Proceedings of SPIE, Volume 11364: Integrated Photonics Platforms: Fundamental Research, Manufacturing and Applications, 113641I (8pp) doi: 10.1117/12.2555762
Type of publication	Conference item
Link to publisher's version	10.1117/12.2555762
Rights	© 2020, Society of Photo-Optical Instrumentation Engineers (SPIE). One print or electronic copy may be made for personal use only. Systematic reproduction and distribution, duplication of any material in this paper for a fee or for commercial purposes, or modification of the content of the paper are prohibited.
Download date	2024-04-18 07:30:33
Item downloaded from	https://hdl.handle.net/10468/12015

UCC
University College Cork, Ireland
Coláiste na hOllscoile Corcaigh

PROCEEDINGS OF SPIE

SPIEDigitalLibrary.org/conference-proceedings-of-spie

Realization of high efficiency ultrasound-powered micro-LEDs for optogenetics

Mondal, Tanmay, Laursen, Kjeld, Hosseini, Seyedsina, Rashidi, Amin, Moradi, Farshad, et al.

Tanmay Mondal, Kjeld Laursen, Seyedsina Hosseini, Amin Rashidi, Farshad Moradi, Brian Corbett, "Realization of high efficiency ultrasound-powered micro-LEDs for optogenetics," Proc. SPIE 11364, Integrated Photonics Platforms: Fundamental Research, Manufacturing and Applications, 113641I (2 April 2020); doi: 10.1117/12.2555762

SPIE.

Event: SPIE Photonics Europe, 2020, Online Only, France

Downloaded From: https://www.spiedigitallibrary.org/conference-proceedings-of-spie on 17 Apr 2020 Terms of Use: https://www.spiedigitallibrary.org/terms-of-use

Realization of high efficiency ultrasound-powered micro-LEDs for optogenetics

Tanmay Mondal *[a], Kjeld Laursen[b], Seyedsina Hosseini[b], Amin Rashidi[b], Farshad Moradi[b], and Brian Corbett[a]

[a]Tyndall National Institute, University College Cork, Cork, Co. Cork, Ireland
[b]Integrated Circuits and Electronics Laboratory, Dept. of Engineering, Aarhus University, Aarhus, Denmark

ABSTRACT

We present the fabrication, characterization, and demonstration of high-efficiency ultrasound-powered micro-light emitting diodes (μLED) for use in optogenetic applications. InGaN based blue-emitting LED material wafers grown on a patterned sapphire substrate (PSS) were used to assist in the out-scattering of the light. The turn-on voltage of the LEDs is around 2.5 volts and the electrical ideality factor is 1.2 confirming high radiative recombination efficiency. A power density of more than 50 mW/mm^2 was obtained from a 130×300 μm^2 LED with a mesa of 100 μm diameter at 3 mA which is much more than is required to excite channelrhodopsin transfected neural cells. A high external quantum efficiency (EQE) of 33% is obtained at 3 mA measured in an integrating sphere. The peak wavelength of the μLED was measured at 483 nm at different current densities. The μLEDs are integrated directly onto a rectifier and Piezoelectric Transducer (PZT) harvester to realise a highly efficient ultrasound-powered light delivery unit capable to generate mWs of optical power. The concept was validated by powering the integrated device with ultrasound.

Keywords: μLED, Ultrasound powering, PZT, Rectifier, Efficiency, Optogenetics, Implantable device

1. INTRODUCTION

Recent technological advancement on implantable devices by combining optics and electronics with genetics has triggered huge interest among researchers.[1,2] The idea of miniaturized electronic ultrasound-powered micro system called the neural DUST has shown promise for future bio-electronics based treatments.[3] We are interested in this method to use in optogenetics[4] and ultra-localized drug delivery system.[4] A previous study showed powerful wireless optoelectronic device on flexible substrate can be used to have complete control over different behavioral patterns.[5] The work presented here is to realize a novel wireless implantable micro-scale device ultimately enabling in-vivo electrophysiology, optogenetics and ultra-localized drug delivery in freely moving animals. The proposed device will be used to target specific neural circuits of the brain and test a new therapeutic approach for Parkinson's disease (PD). The device is based on highly efficient ultrasound powered micro-scale light emitting diodes (μLEDs) which will be used to excite specific channelrhodopsin transfected neural cells.

The proposed DUST size needs to be in the sub-millimeter range and to be energised at a centimeter or so below the skin. A much larger implant was shown in[6] where a fully integrated ultrasound-powered electrical device capable of operating 10.5 cm below the skin. The DUST needs to generate 1-20 mW/mm^2 of optical power at 1 mA and needs to result in less than 1 K temperature rise to prevent damage of cells. The peak wavelength should be around 480 nm which is suited to excite channelrhodopsin transfected cells.[7,8]

The piezoelectric element (PZT) used here was a cube of $(500\ \mu m)^3$ and the rectifier chip had dimensions of $(300\ \mu m)^3$. The rectifier chip had four Aluminium (Al) pads each having dimensions of 50×100 μm^2. The μLED is integrated on the output of the active bridge rectifier. The rectifier harvests the AC power generated by the PZT crystal and then converts it in to DC power to the μLED.

Further author information: (Send correspondence to tanmay.mondal@tyndall.ie)
Tanmay Mondal: E-mail: tanmay.mondal@tyndall.ie, Telephone: +353 21 234 6519

Integrated Photonics Platforms: Fundamental Research, Manufacturing and Applications, edited by Roel G. Baets, Peter O'Brien, Laurent Vivien, Proc. of SPIE Vol. 11364, 113641I
© 2020 SPIE · CCC code: 0277-786X/20/$21 · doi: 10.1117/12.2555762

Downloaded From: https://www.spiedigitallibrary.org/conference-proceedings-of-spie on 17 Apr 2020
Terms of Use: https://www.spiedigitallibrary.org/terms-of-use

Several studies has been made on the efficiency of InGaN based blue μLEDs.[9–11] The efficiency the the LED is generally higher at low currents and then falls off with increasing current densities. This droop phenomenon is due to different recombination and leakage mechanisms inside the epitaxial structure such as leakage via structural defects,[12] Auger recombination,[13] and the effect of built-in piezo-electric fields in quantum wells (QW).[14] In this work the fabricated μLED had an external quantum efficiency of 33% at 3 mA while the wall-plug efficiency was 37%.

2. DESIGN AND FABRICATION OF MICRO-LED

2.1 Mask design

The μLED ultimately to be flip-chip mounted on the rectifier chip that has two aluminium pads of size 50×100 μm^2 each with a 200 μm gap between the pads. Based on the design of the rectifier chip, the μLED can be maximum of 330 μm long and 150 μm wide. A mask was designed to fabricate the μLED matching the dimensions of the rectifier chips. The mask contains the design of μLEDs with different shape and mesa size as the performance of the μLED with variation of physical dimensions could be assessed.

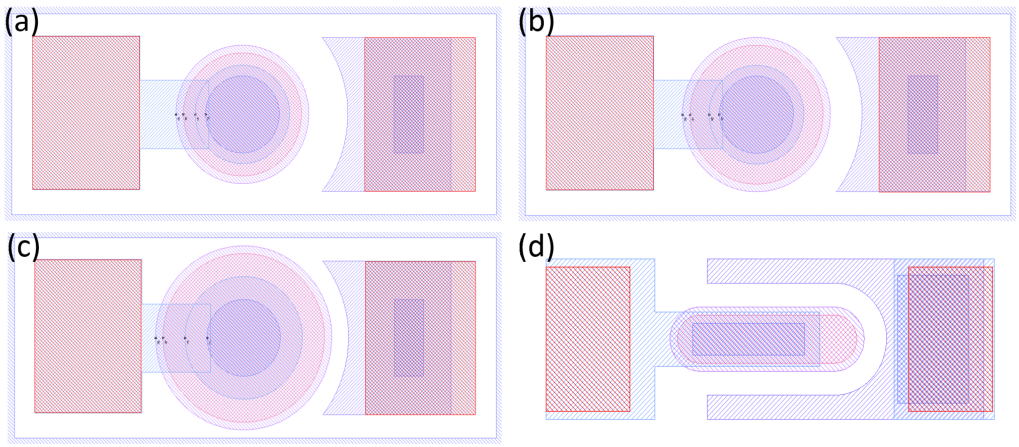

Figure 1. μLEDs of different mesa shape and size while matching the dimensions of the active bridge rectifier. (a) Circular mesa, diameter 90 μm, area 6362 μm^2, (b) Circular mesa, diameter 100 μm, area 7854 μm^2, (c) Circular mesa, diameter 120 μm, area 11310 μm^2 and (d) Cigar shaped mesa, area 4852 μm^2.

2.2 μLED fabrication

To fabricate the μLED, InGaN quantum well based blue LED wafer grown on patterned sapphire substrate (PSS) was used. It has been experimentally verified that PSS assists out-scattering of light which increases the extraction efficiency of the LED.

The wafer was cleaned first with organic, acid and base solutions. The process flow is shown in Fig 2: First the p-metal was defined by lift-off lithography. Pd: Ni: Au with thickness of 10: 20: 30 nm deposited. Then a mesa was defined and etched 1.2 μm deep by Inductive Coupled Plasma (ICP) etching Cl_2. A third lithography step was used to define the n-contact metal. Ti: Al: Ti: Au = 20: 170: 50: 100 nm was deposited for this purpose. Then the surface was passivated by depositing 295 nm of SiO_2 by sputtering. Then a patterned oxide etch was done to open sections for bond pads. A final lithography was done for bond pad metal comprising of Ti: Au = 20: 200 nm.

2.3 Backend processing

The thickness of the PSS wafer was 350 μm. Boron Carbide was used to grind the sapphire substrate and thin it down to 110 μm. Finally, the back surface was semi polished by 9 μm Al_2O_3 powder and SF1 polishing solution.

Downloaded From: https://www.spiedigitallibrary.org/conference-proceedings-of-spie on 17 Apr 2020
Terms of Use: https://www.spiedigitallibrary.org/terms-of-use

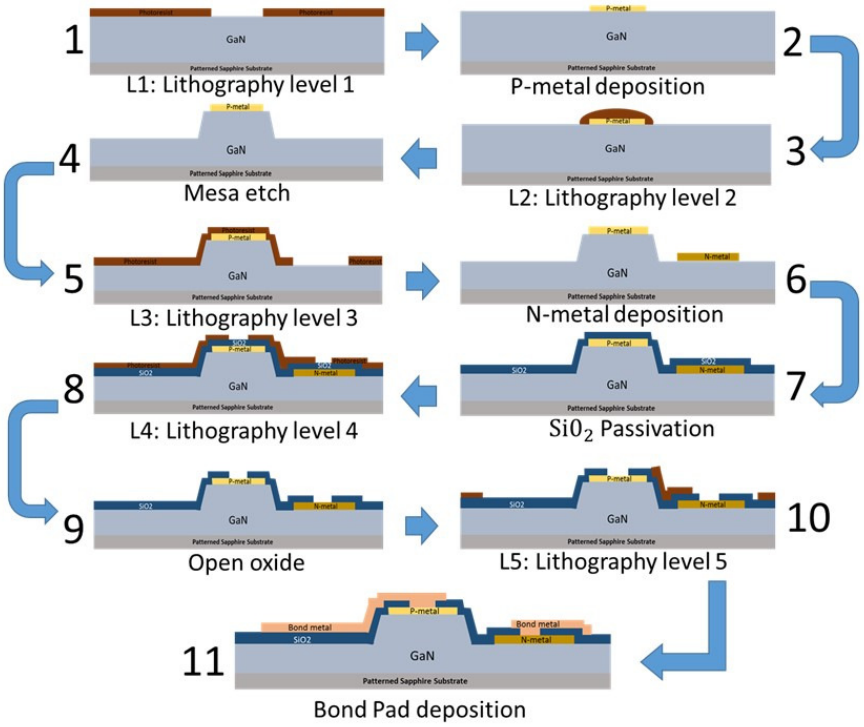

Figure 2. μLED fabrication steps.

Further improvement on extraction efficiency was achieved by sputtering 83 nm of SiO_2 on the semi polished sapphire substrate as anti-reflection coating (ARC).

The μLEDs were then diced into individual chips of size 130×300 μm^2 to permit stud bumping onto contact pads .

3. CHARACTERIZATION

Achieving high quality ohmic contact between p-metal and p-GaN has always been one of the key issues relating to GaN based LEDs. Specific contact resistivity (ρ_c) can be extracted from a circular transmission line measurement (c-TLM) arrangement using the following equation,

$$R_{pp} = \frac{R_{sh}}{2\pi} ln \frac{r_0}{r_i} + \frac{\rho_c}{2\pi L_s} (\frac{1}{r_0} + \frac{1}{r_i}), \quad (1)$$

where R_{sh} is the sheet resistance, L_s is current spreading length, R_{pp} is the point-to-point resistance and r_0, r_i defines the outer and inner radius of the cTLM. The ρ_c was determined using the data presented in Fig. 3 and then fitting the data in Equation 1 (Fig. 4). A high quality ohmic contact with specific contact resistivity of the order of 10^{-4} Ωcm^2 has been obtained.

The electrical and optical performance of the μLEDs were then assessed based on the difference of mesa diameters. 2.5 V was found to be the turn on voltage of the μLEDs by current-voltage (I-V) characteristics measurement. For 100 μm diameter mesa LEDs, the electrical ideality factor (η) reaches a very low value of 1.2 at 2.3 volts, indicating highly efficient radiative recombination (Fig. 5).

A comparison between different mesa sizes and shapes μLEDs is made (Fig. 6). It is demonstrated that EQE also depends on the size of the LEDs. The largest mesa LED (120 μm diameter) has the highest external quantum efficiency (EQE). The smaller devices (cigar shaped and 90 μm diameter mesa) have lower EQE. Based

Downloaded From: https://www.spiedigitallibrary.org/conference-proceedings-of-spie on 17 Apr 2020
Terms of Use: https://www.spiedigitallibrary.org/terms-of-use

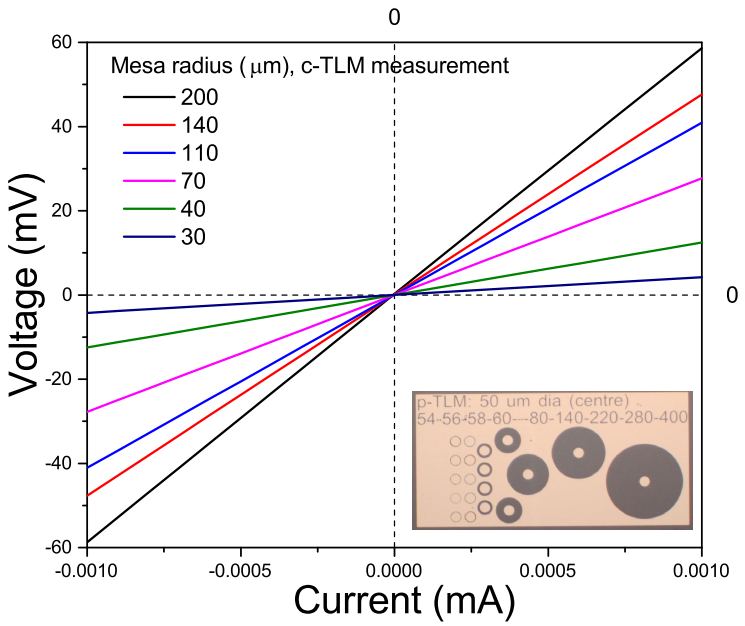

Figure 3. I-V measurement on c-TLMs.

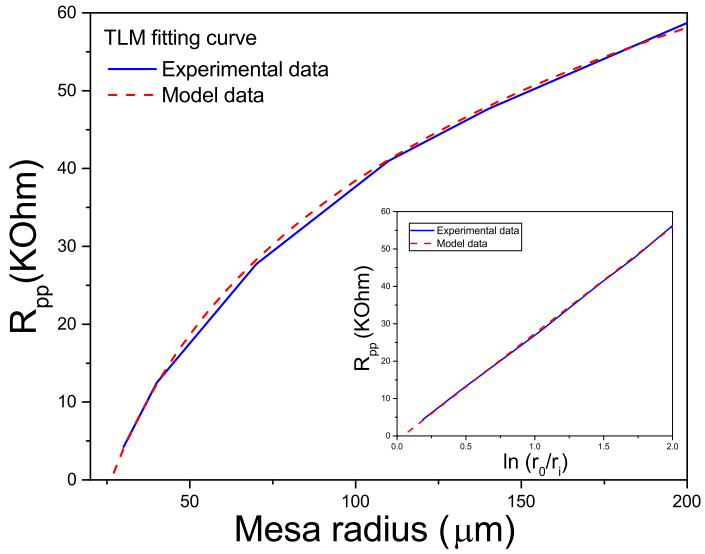

Figure 4. TLM fitting curve with respect to point to point resistance (R_{pp}) .

on these measurements of the ideality factor, I-V characteristics and contact resistivity, it has been determined that 100 μm mesa diameter μLED will be the best suited for this application.

An output optical power of more than 1.5 mW was measured at 3 mA when the μLED was placed directly on top of the detector. This represents collection of all the light that is coming out from the bottom of the μLED and has a numerical aperture (NA) = 1. A power density of 190 mW/mm^2 was obtained in this situation.

$$I = I_0 exp(\frac{qV}{\eta KT}), \tag{2}$$

The EQE of an LED refers to the number of extracted photons from the LED due to injection of electrons

Downloaded From: https://www.spiedigitallibrary.org/conference-proceedings-of-spie on 17 Apr 2020
Terms of Use: https://www.spiedigitallibrary.org/terms-of-use

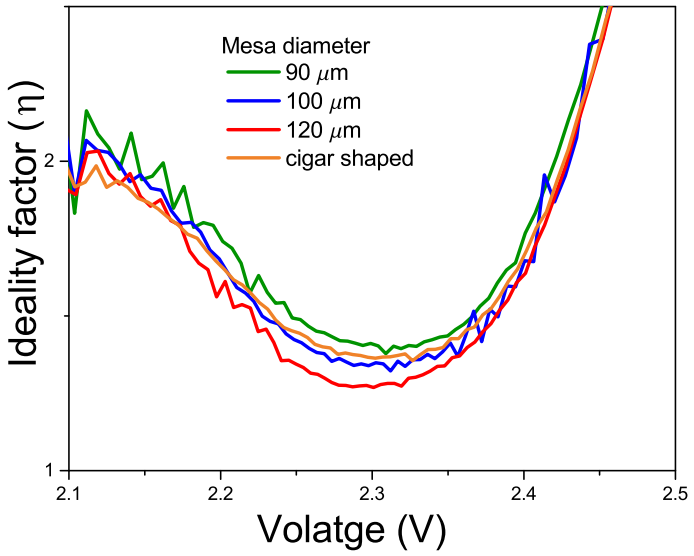

Figure 5. Measure of the ideality factor with respect to voltage.

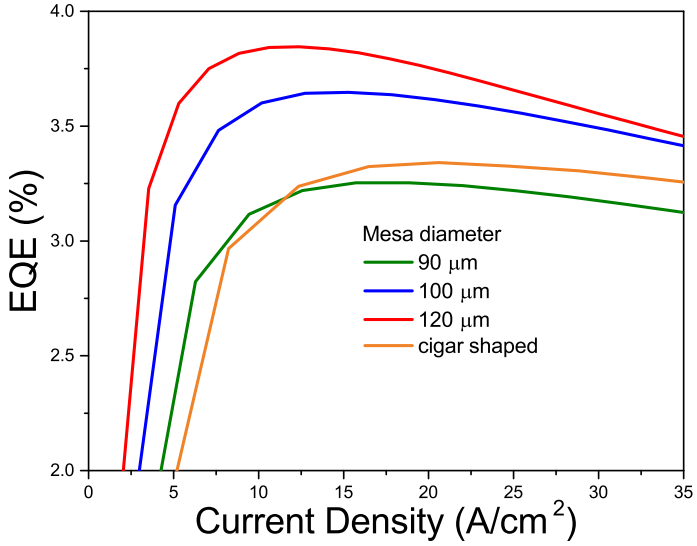

Figure 6. Measure of the external quantum efficiency at a solid angle of emission of $\pm 30^{\circ}$ as a function of current density with variation of mesa size.

and is represented by the following equation:

$$EQE = \frac{P_{photo}}{I} \frac{1}{\frac{hc}{\lambda}}, \tag{3}$$

There is additional light coming out from the sides of the mesa which needs to be taken account to assess the ultimate EQE of the μLED. An output power of more than 2.5 mW was measured at 3 mA in an integrating sphere. By embedding the LED inside an index matched fluid such as epoxy we can expect an additional 8% light output.

Fig. 7 represents the comparison of EQE of the μLED when it is placed directly on top of the detector (NA=1) and when measured in an integrating sphere.

Downloaded From: https://www.spiedigitallibrary.org/conference-proceedings-of-spie on 17 Apr 2020
Terms of Use: https://www.spiedigitallibrary.org/terms-of-use

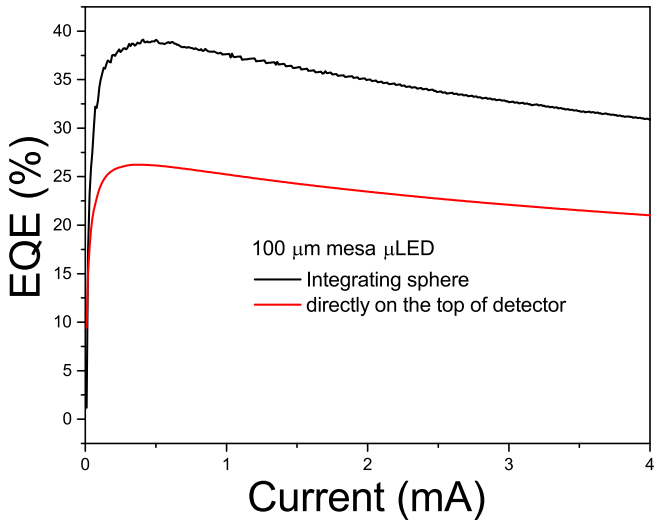

Figure 7. External Quantum Efficiency (EQE) with respect to bias current.

An EQE of about 23% at 3 mA was obtained at NA=1, while about 33% at 3 mA when measured in integrating sphere. About 0.94 mW of integrated output power was measured at 1 mA referring to a high wall-plug efficiency of 37%.

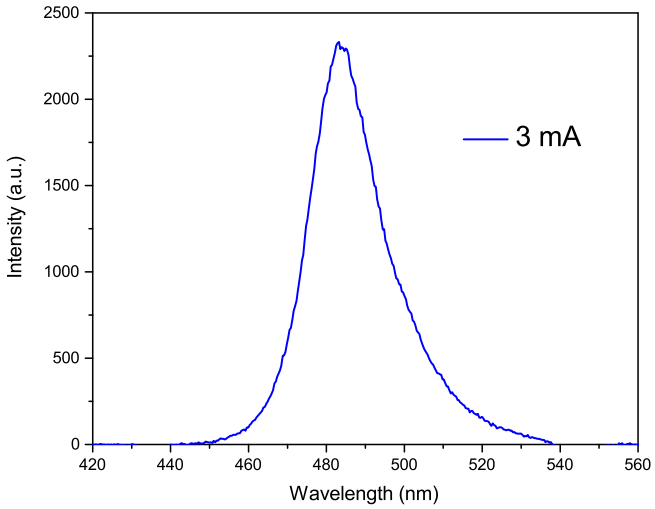

Figure 8. Electroluminescence spectra of the 100 μm mesa LED.

Fig. 8 represents the electroluminescence (EL) spectrum of the 100 μm diameter mesa LED with respect to bias current. The peak wavelength is obtained at 483 nm which is required for the excitation of the channelrhodopsin transfected cells.

4. DUST PROTOTYPE INTEGRATION

The final step in this work is to integrate all the components to complete the DUST prototype. Each individual component comes with its own limitations and requirements. The PZT crystal is susceptible to exposure to

Downloaded From: https://www.spiedigitallibrary.org/conference-proceedings-of-spie on 17 Apr 2020
Terms of Use: https://www.spiedigitallibrary.org/terms-of-use

temperatures of over 110 degrees and has silver (Ag) contact pads on the top and bottom surface. The bridge rectifier has four Al pads which creates aluminium oxide layers when exposed in uncontrolled environment. The pads are also recessed by 3 μm compared to the other areas of the rectifier. Also, the rectifier does not come with any kind of ESD protection.

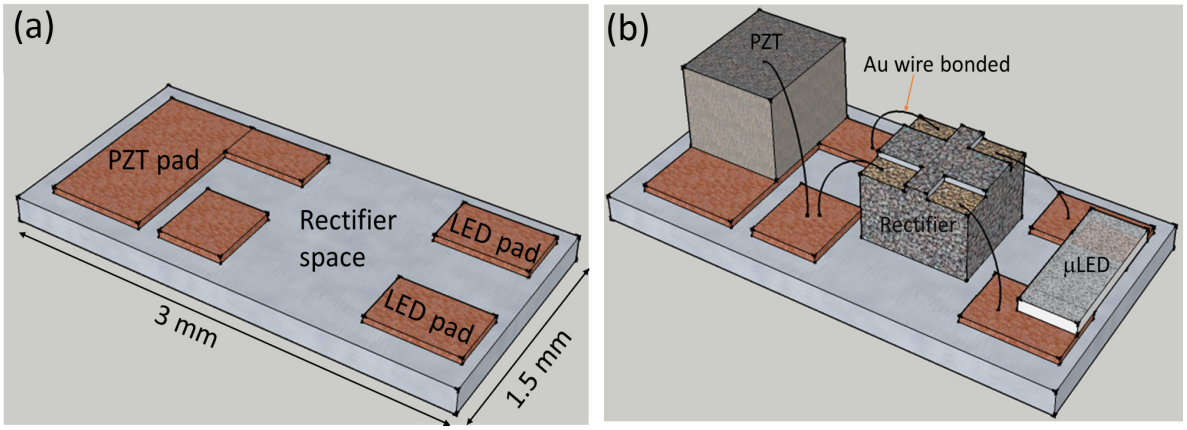

Figure 9. Schematics of (a) fabricated submount and (b) integrated prototype.

A process was developed in order to prepare a submount for the DUST prototype. Patterned Ti: Au =20: 200 nm was deposited on to a 500 μm thick glass substrate to produce the submount and then the glass wafer was diced into 1.5 mm $\times$ 3.0 mm individual pieces. The submount has two pads of dimension of 500$\times$500 μm^2 for the μLED, one 1 mm^2 pad for the PZT crystal and one open space for rectifier integration (Fig. 9(a)).

First the μLED was integrated to the submount as it is the most robust component. First, two gold studs were made on each of the μLED pads of the sub-mount and then solder bump was deposited on them. The studs were then flattened by a smooth silicon piece. Similarly, one gold stud was deposited on each of the μLED pads and flattened. The μLED was then bonded to the submount using a flip-chip bonder using thermal compression at 270 degrees for 20 seconds. A small amount of non-conductive epoxy was used on the edges of the μLED to strongly hold it to the submount.

The PZT crystal was then bonded to the submount by using room temperature-curable silver epoxy which was left to harden. The bridge rectifier was glued to the open space of the submount by non-conductive epoxy by taking precautions needed for non-ESD protected chip. The interconnection between the devices was made by Au wire bonding and finally all the Au bonded sections were secured by non-conductive epoxy (Fig. 9(b)). Finally, the integrated device was encapsulated by spin coating of thin layer of polydimethylsiloxane (PDMS). PDMS was chosen because of its bio-compatibility and acoustic impedance matching between tissue and water.

5. PROTOTYPE DEMONSTRATION

In order to demonstrate the encapsulated prototype it was first mounted on to a PCB. Then submerged into water, oriented so it faces the ultrasound transducer. An acoustic intensity of 7.2 mW/mm^2 at a frequency of 3.14 MHz was delivered to the PZT crystal. As the prototype is completely electrically isolated, the acoustic power transfer was observed visually by the blinking of the μLED. The ultrasonic power was duty cycled at a repetition cycle of 1 Hz.

6. CONCLUSION

In this paper we have successfully demonstrated a prototype ultrasound-powered DUST with the integration of a 37% wall-plug efficiency μLED to an active bridge rectifier and PZT crystal. This proves that the approach is feasible and can perform well.

Downloaded From: https://www.spiedigitallibrary.org/conference-proceedings-of-spie on 17 Apr 2020
Terms of Use: https://www.spiedigitallibrary.org/terms-of-use

In future, further miniaturisation of the μLED along with the DUST will be performed. Methods have been developed to produce 5 μm thick μLEDs. We will also target compact integration of both blue and red μLEDs on to a single chip with improved rectifier and PZT to implant on freely moving animals.

ACKNOWLEDGMENTS

This project (STARDUST) has received funding from the European Union Horizon 2020 research and innovation program under grant agreement No 767092. The authors would like to acknowledge Noreen Nudds and Junsu lee for their assistance with device integration.

REFERENCES

[1] Delivopoulos, E., Chew, D. J., Minev, I. R., Fawcett, J. W., and Lacour, S. P., "Concurrent recordings of bladder afferents from multiple nerves using a microfabricated pdms microchannel electrode array," *Lab on a chip* **12**(14), 2540–2551 (2012).

[2] Boretius, T., Badia, J., Pascual-Font, A., Schuettler, M., Navarro, X., Yoshida, K., and Stieglitz, T., "A transverse intrafascicular multichannel electrode (time) to interface with the peripheral nerve," *Biosensors and Bioelectronics* **26**(1), 62–69 (2010).

[3] Seo, D., Neely, R. M., Shen, K., Singhal, U., Alon, E., Rabaey, J. M., Carmena, J. M., and Maharbiz, M. M., "Wireless recording in the peripheral nervous system with ultrasonic neural dust," *Neuron* **91**(3), 529 – 539 (2016).

[4] il Kim, T., McCall, J. G., Jung, Y. H., Huang, X., Siuda, E. R., Li, Y., Song, J., Song, Y. M., Pao, H. A., Kim, R.-H., Lu, C., Lee, S. D., Song, I.-S., Shin, G., Al-Hasani, R., Kim, S., Tan, M. P., Huang, Y., Omenetto, F. G., Rogers, J. A., and Bruchas, M. R., "Injectable, cellular-scale optoelectronics with applications for wireless optogenetics," *Science* **340**(6129), 211–216 (2013).

[5] Shin, G., Gomez, A. M., Al-Hasani, R., Jeong, Y. R., Kim, J., Xie, Z., Banks, A., Lee, S. M., Han, S. Y., Yoo, C. J., Lee, J.-L., Lee, S. H., Kurniawan, J., Tureb, J., Guo, Z., Yoon, J., Park, S.-I., Bang, S. Y., Nam, Y., Walicki, M. C., Samineni, V. K., Mickle, A. D., Lee, K., Heo, S. Y., McCall, J. G., Pan, T., Wang, L., Feng, X., il Kim, T., Kim, J. K., Li, Y., Huang, Y., Gereau, R. W., Ha, J. S., Bruchas, M. R., and Rogers, J. A., "Flexible near-field wireless optoelectronics as subdermal implants for broad applications in optogenetics," *Neuron* **93**(3), 509 – 521.e3 (2017).

[6] Charthad, J., Chang, T. C., Liu, Z., Sawaby, A., Weber, M. J., Baker, S., Gore, F., Felt, S. A., and Arbabian, A., "A mm-sized wireless implantable device for electrical stimulation of peripheral nerves," *IEEE Transactions on Biomedical Circuits and Systems* **12**(2), 257–270 (2018).

[7] Nagel, G., Brauner, M., Liewald, J. F., Adeishvili, N., Bamberg, E., and Gottschalk, A., "Light activation of channelrhodopsin-2 in excitable cells of caenorhabditis elegans triggers rapid behavioral responses," *Current Biology* **15**(24), 2279–2284 (2005).

[8] Nagel, G., Szellas, T., Kateriya, S., Adeishvili, N., Hegemann, P., and Bamberg, E., "Channelrhodopsins: directly light-gated cation channels," *Biochemical Society Transactions* **33**(4), 863–866 (2005).

[9] Hwang, D., Mughal, A., Pynn, C. D., Nakamura, S., and DenBaars, S. P., "Sustained high external quantum efficiency in ultrasmall blue iii–nitride micro-leds," *Applied Physics Express* **10**(3), 032101 (2017).

[10] Jia, X., Zhou, Y., Liu, B., Lu, H., Xie, Z., Zhang, R., and Zheng, Y., "A simulation study on the enhancement of the efficiency of gan-based blue light-emitting diodes at low current density for micro-led applications," *Materials Research Express* **6**(10), 105915 (2019).

[11] Tian, P., McKendry, J. J., Gong, Z., Guilhabert, B., Watson, I. M., Gu, E., Chen, Z., Zhang, G., and Dawson, M. D., "Size-dependent efficiency and efficiency droop of blue ingan micro-light emitting diodes," *Applied Physics Letters* **101**(23), 231110 (2012).

[12] Eliseev, P. G., Osin'ski, M., Li, H., and Akimova, I. V., "Recombination balance in green-light-emitting gan/ingan/algan quantum wells," *Applied Physics Letters* **75**(24), 3838–3840 (1999).

[13] Shen, Y., Mueller, G., Watanabe, S., Gardner, N., Munkholm, A., and Krames, M., "Auger recombination in ingan measured by photoluminescence," *Applied Physics Letters* **91**(14), 141101 (2007).

[14] Kim, M.-H., Schubert, M. F., Dai, Q., Kim, J. K., Schubert, E. F., Piprek, J., and Park, Y., "Origin of efficiency droop in gan-based light-emitting diodes," *Applied Physics Letters* **91**(18), 183507 (2007).

Downloaded From: https://www.spiedigitallibrary.org/conference-proceedings-of-spie on 17 Apr 2020
Terms of Use: https://www.spiedigitallibrary.org/terms-of-use